ORIGINAL ARTICLE
Iran J Allergy Asthma Immunol
February 2026; 25(1):93-107.
DOI: 10.18502/ijaai.v25i1.20442

Development and Validation of a Manganese-metabolism and Immune-integrated Gene Signature for Prognosis and Immune Contexture in Patients with Colorectal Cancer

Lei He[1], Zhengxin Chen[1], Chang Zhang[1], Panyu Zhu[2], and Shiming Dai[3]

[1] Department of Anorectal, Nanjing Hospital of Chinese Medicine Affiliated to Nanjing University of Chinese Medicine, Nanjing, China
[2] Internal Medicine of Traditional Chinese Medicine (Endocrine Diseases), Nanjing Hospital of Chinese Medicine Affiliated to Nanjing University of Chinese Medicine, Jiangsu, China
[3] Department of General Surgery, Nanjing Hospital of Chinese Medicine Affiliated to Nanjing University of Chinese Medicine, Nanjing, China

Received: 1 July 2025; Received in revised form: 9 September 2025; Accepted: 19 September 2025

ABSTRACT

Colorectal cancer (CRC) is the third most frequently diagnosed cancer and the second leading cause of cancer-related mortality globally. Emerging evidence identifies manganese as an important trigger for the cyclic GMP-AMP synthase (cGAS)-stimulator of interferon genes (STING) pathway, but prognostic signatures integrating manganese metabolism and immune pathways remain unexplored in CRC.

Through analysis of transcriptomic and clinical data from TCGA-CRC and GSE17538 cohorts, we established and validated an eleven-gene manganese metabolism and immune-related signature that robustly stratified CRC patients into distinct risk groups with significant survival differences.

High-risk patients exhibited suppressed immune microenvironments with enriched M2 macrophages and Tregs and activation of oncogenic pathways. Quantitative real-time polymerase chain reaction (qRT-PCR) validation confirmed dysregulation of eight signature genes in clinical CRC samples, indicating the model's potential for prognostic prediction and immunotherapeutic stratification.

We established a novel MIRGs signature that accurately predicts CRC clinical outcome. Integration of manganese-based agents with immune checkpoint inhibitors (ICIs) represents a potential therapeutic strategy for immunotherapy-resistant CRC.

Keywords: Colorectal cancer; Immunotherapy resistance; Manganese metabolism; Prognosis

Corresponding Author: Shiming Dai, MD.
Department of General Surgery, Nanjing Hospital of Chinese Medicine Affiliated to Nanjing University of Chinese Medicine, Nanjing, China. Tel: (+86 025) 8636 9061, Fax: (+86 025) 8636 9061 Email: 312747216@qq.com

Lei He and Zhengxin Chen contributed equally to this study.

INTRODUCTION

Colorectal cancer (CRC) is the third most frequently diagnosed cancer and the second leading cause of cancer mortality, representing a substantial health issue.[1,2] Despite advances in surgical techniques and systemic

therapies, including chemotherapy, targeted agents, and immunotherapy, outcomes for advanced disease remain suboptimal due to intrinsic and acquired resistance mechanisms.[3,4] Immune checkpoint inhibitors (ICIs), especially those that target PD-1/PD-L1, have proven clinically effective in CRC patients with microsatellite instability-high (MSI-H).[5,6] However, tumors that are microsatellite stable (MSS), which constitute the majority, have restricted response rates.[7] This underscores the critical need to identify novel mechanisms to overcome immunotherapy resistance.

Evidence from recent studies emphasizes the significant involvement of the cGAS-STING pathway in antitumor immunity through the detection of cytosolic DNA and the activation of type I interferon production.[8,9] Manganese (Mn^{2+}) functions as a potent cGAS-STING activator, enhancing STING palmitoylation and downstream TBK1-IRF3 signaling.[10,11] Preclinical studies demonstrate that Mn^{2+} augments dendritic cell maturation, promotes cytotoxic T lymphocyte infiltration, and synergizes with ICIs to suppress tumor growth across multiple cancer models.[10,12] Furthermore, Mn^{2+} deficiency compromises antitumor immunity, while Mn^{2+} supplementation restores immune surveillance.[13,14] This positions manganese metabolism as a critical modulator of the tumor immune microenvironment.

Given this central role of manganese in immune regulation, we hypothesized that manganese metabolism-related genes (MRGs) may synergize with immune-related genes (IRGs) to influence tumor behavior and patient outcomes. While many prognostic signatures for CRC have focused on IRGs,[15,16] the influence of essential micronutrient metabolism on immune function is often overlooked. The interplay between MRGs and IRGs remains unexplored in CRC prognostication. Integrating these dimensions could yield more comprehensive biomarkers reflecting both immune activation capacity and metabolic reprogramming within the tumor microenvironment.

The purpose of this study was to identify differentially expressed MRGs and IRGs between colorectal tumor tissues and normal tissues and construct a manganese metabolism- and immune-related gene signature (MIRGs) for predicting prognosis. We further evaluated the association of MIRG subtypes with the tumor immune microenvironment, the response to immunotherapy, and validated the expression levels of key signature genes in colorectal clinical samples. Our integrated approach could provide novel insights into CRC biology and deliver a clinically applicable method for risk stratification and treatment personalization.

MATERIALS AND METHODS

Data Sources and Processing

Clinical data and RNA sequencing profiles for CRC were retrieved from the Gene Expression Omnibus (GEO) and The Cancer Genome Atlas (TCGA) databases. The TCGA-CRC database, obtained from UCSC XENA (https://xenabrowser.net/datapages/), was used as the training cohort, while the GSE17538 database from GEO (http://www.ncbi.nlm.nih.gov/geo/) was employed as the validation cohort. Batch effects between databases were mitigated using the sva R package. Specifically, the ComBat algorithm (default parameters) was applied to harmonize the expression data from TCGA and GEO datasets. Principal component analysis (PCA) was performed before and after correction, confirming that the batch effect was markedly reduced after ComBat adjustment. Patients were excluded if they had missing survival or clinical information, or if their overall survival was less than 30 days to avoid bias from perioperative mortality. After excluding samples lacking survival data or containing incomplete clinical information, the final cohorts comprised 315 TCGA-CRC samples and 298 GSE17538 samples. The flowchart displaying the entire research was shown in Figure 1.

Identification of Differentially Expressed Genes Associated with Manganese Metabolism and Immune Function

A curated set of manganese metabolism-related genes was retrieved from GeneCards (https://www.genecards.org/). Immune-related genes were retrieved from the ImmPort database (https://www.immport.org/). Using the edgeR R package, differential expression analysis was carried out on colorectal tumor tissues and adjacent normal tissues from the TCGA-COAD dataset and GEO database. Differentially expressed genes (DEGs) were determined by an absolute log2 fold change (|log2FC|)> 1 and an adjusted *p* value<0.05. Subsequent screening focused on DEGs intersecting with the manganese metabolism- and immune-related gene lists.

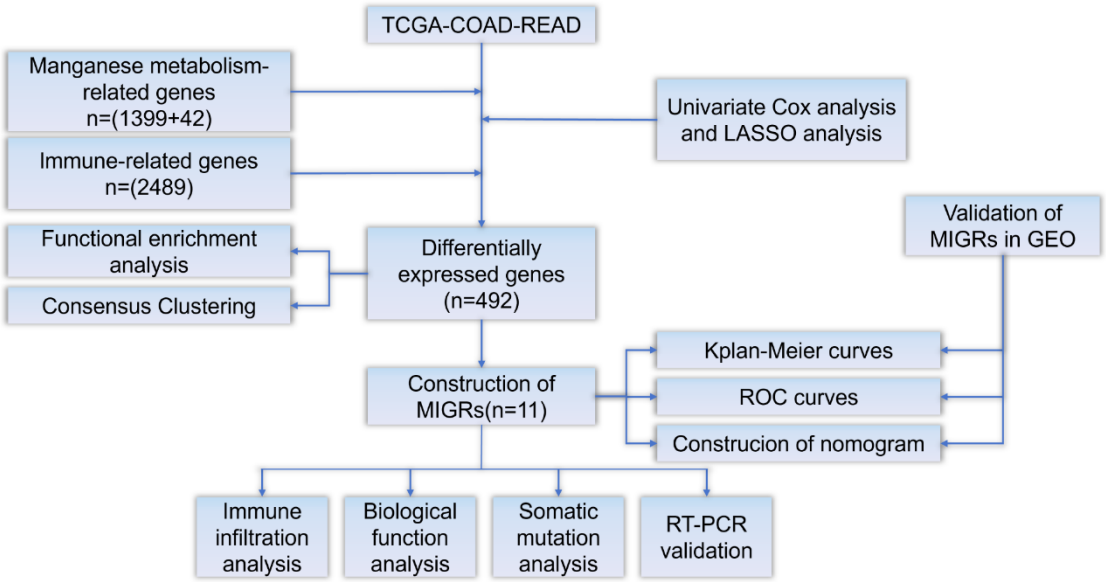

Figure 1. The flowchart displaying the entire research.

Functional Enrichment Analysis

The clusterProfiler R package was used to analyze the identified DEGs related to manganese metabolism and immunity via Kyoto Encyclopedia of Genes and Genomes (KEGG) pathway enrichment analysis and Gene Ontology (GO) annotation, encompassing Biological Process (BP), Molecular Function (MF), and Cellular Component (CC) categories.

Unsupervised Clustering Based on DEGs Associated with Immune and Manganese Metabolism

Using the NMF R package, consensus clustering of the TCGA-CRC cohort was conducted based on the expression profiles of DEGs related to manganese metabolism and immunity using the NMF algorithm, which is particularly suitable for non-negative gene expression data and provides biologically interpretable clustering results. To determine the optimal cluster number, we evaluated cophenetic correlation coefficients and silhouette widths across k=2–6. Both metrics consistently indicated k=3 as the most stable solution. Kaplan-Meier survival curves and log-rank tests were used to evaluate differences in overall survival (OS) between subtypes. For each subtype, the ESTIMATE algorithm was used to calculate stromal, immune, and ESTIMATE scores, as well as tumor purity. The Wilcoxon rank-sum tests were used to compare the expression levels of immune checkpoint genes across different subtypes. Gene Set Variation Analysis (GSVA) interrogated enrichment pathway differences among subtypes.

Construction and Verification of MIRGs

The identification of OS-associated genes in the TCGA-CRC cohort was achieved through univariate Cox regression, with LASSO Cox regression refining the prognostic signature. A 10-fold cross-validation strategy was employed to determine the optimal penalty parameter (λ), which balances model complexity and predictive accuracy and minimizes overfitting. The risk score was determined by the formula: RiskScore = Σ^{n}_{i} coefficient × Expression (X_i) for each gene in the signature. Patients were classified into high- and low-risk groups using the median risk score. Kaplan-Meier analysis and ROC curves were used to validate the prognostic performance. The signature was independently tested in the GSE17538 cohort. Univariate or multivariate Cox regression evaluated clinical independence.

Establishment of a Nomogram

To estimate 12-, 24-, and 36-month survival, a clinical nomogram was formulated by integrating risk scores and clinicopathological variables using the rms package. Calibration curves and ROC analysis assessed predictive accuracy.

Evaluation of the Tumor Microenvironment

CIBERSORT was used to measure the infiltration of immune cells, while ssGSEA (GSVA, GSEABase) was used to assess the enrichment of immunological functions. Wilcoxon tests were used to compare immune characteristics between different risk groups.

Performing Gene Set Variation Analysis on MIRGs

Hallmark gene sets were employed by the GSVA package to assess pathway activity differences between risk subgroups.

Tumor Mutation Burden Analysis

TMB was defined as mutations per megabase. Somatic mutations were visualized using waterfall plots. Mutation type distributions were compared between risk groups.

Clinical Tissue Samples

Fifty paired CRC and adjacent non-tumor tissues were collected from retrospective surgical specimens. Tissues were pathologically confirmed, paraffin-embedded, or cryopreserved at −80 °C. Written informed consent was obtained under Institutional Ethics Committee approval. This study obtained approval from the independent Ethics Committee of Nanjing Hospital of Chinese Medicine, affiliated with Nanjing University of Chinese Medicine (KY2024010).

RNA Isolation and Quantitative Real-time PCR (qRT-PCR)

TRIzol reagent (Invitrogen) was used to extract total RNA. cDNA was generated from 1 μg of RNA using the PrimeScript RT kit (Takara). SYBR Green assays (Takara) were employed for RT-qPCR on a CFX-96 system (Bio-Rad), and relative expression was determined using the $2^{-\Delta\Delta Ct}$ method normalized to GAPDH. The experiment included three independent biological replicates, each with technical triplicates.

Statistical Analysis

Analyses used R v4.3.0 and GraphPad Prism v8.0.2. Continuous variables were compared by Student's t-test (normal distribution) or Wilcoxon test (non-normal). Multiple groups were assessed via the Kruskal-Wallis test. The Spearman method was used for correlations, and data are presented as mean ± SD. Statistical significance was indicated by $p<0.05$.

RESULTS

Identification of Differentially Expressed Genes Associated with Manganese Metabolism and Immune Function

To ensure comparability across datasets, batch effects between TCGA and GEO were removed using the ComBat algorithm. PCA confirmed that, after ComBat correction, the distributions of samples were primarily driven by biological features rather than dataset origin, indicating successful batch-effect removal. A total of 2861 genes showed differential expression between CRC and normal tissues according to the initial screening of the TCGA database (Figure 2A). We concentrated our study on 492 genes that are functionally associated with manganese metabolism and immune functions (Figure 2B). Significant enrichment in immune activation pathways, including cytokine-cytokine receptor interaction, chemokine signaling pathway, viral protein interaction with cytokine and cytokine receptor, hormone signaling, and the IL-17 signaling pathway, was demonstrated by KEGG functional annotation (Figure 2C). The enrichment of pathways such as IL-17 signaling and cytokine-cytokine receptor interaction is consistent with the established role of chronic inflammation and immune cell crosstalk in colorectal carcinogenesis and progression. Further insights from GO functional annotation analysis showed that genes involved in manganese metabolism and immune response are mainly active in certain biological processes. These processes encompass leukocyte migration and leukocyte chemotaxis. For molecular functions, they participate in cytokine activity and cytokine receptor binding. Regarding cellular components, they localize to secretory granule lumen. The bar plot in Figure 2D illustrates the eight most significant terms within the categories of Biological Process (BP), Molecular Function (MF), and Cellular Component (CC).

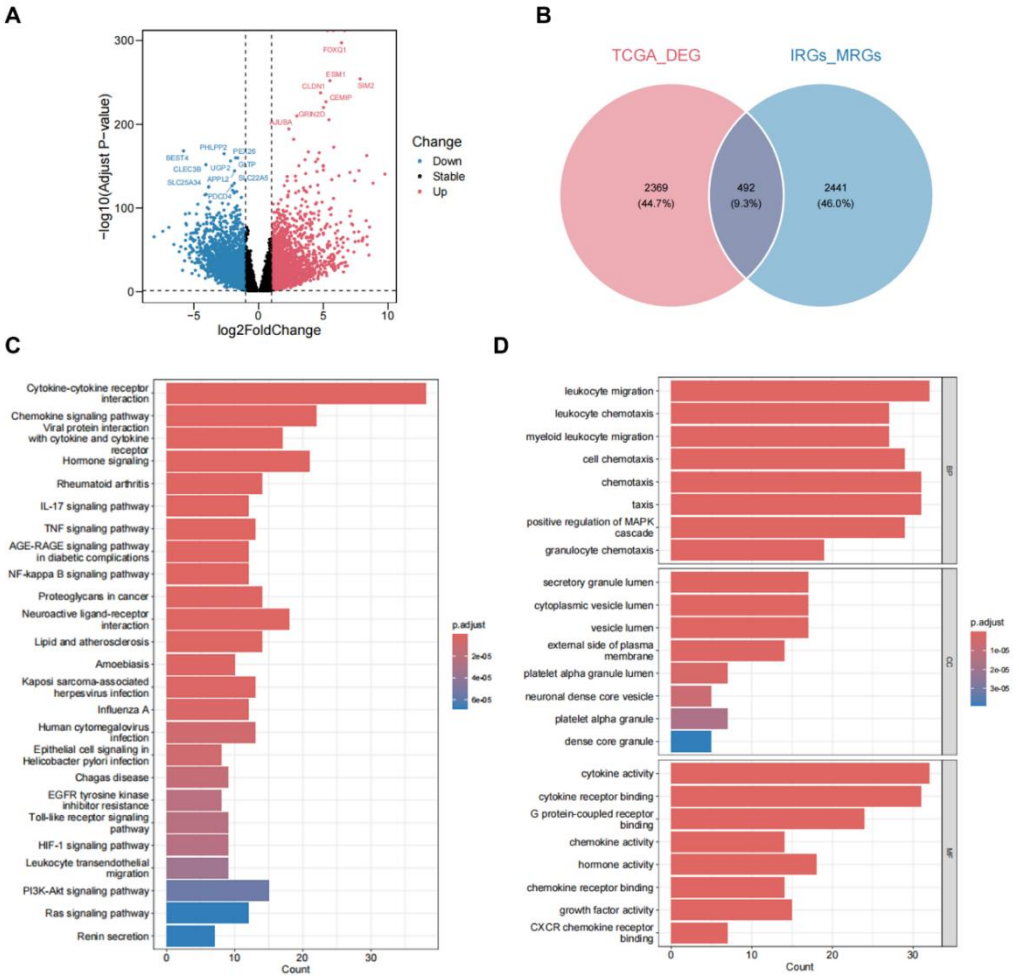

Figure 2. Gene screening and functional enrichment analysis. A. The Cancer Genome Atlas (TCGA) dataset-derived volcano plot illustrating differentially expressed denes (DEGs) in colorectal cancer. B. Venn diagram identifying 492 co-differentially expressed metabolism-related genes (MRGs) and immuno-related genes (IRGs). C, D. Bar graph presenting Kyoto Encyclopedia of Genes and Genomes (KEGG) pathway enrichment (C) and Gene Ontology (GO) functional enrichment (D) results for these 492 genes.

Establishment of Three Subtypes Through Unsupervised Clustering

The entire cohort was segmented into three subtypes (clusters 1–3) using NMF-based consensus clustering. This method was chosen due to its suitability for gene expression data and interpretability of non-negative factors. Evaluation of clustering stability using cophenetic correlation and silhouette width confirmed that the three-cluster solution was the most robust and biologically meaningful (Figure 3A). In addition, our investigation into the prognostic differences among these three subtypes demonstrated a statistically significant disparity in overall survival outcomes (p=0.033, Figure 3B). Compared to the other clusters, Cluster 2 showed longer overall survival times than the other clusters, indicating a better prognosis for Cluster 2. Examination of tumor microenvironment heterogeneity across subtypes is presented in Figures 3C-F. The immunological and ESTIMATE scores in cluster 2 were significantly lower than those in the other clusters, and its tumor purity was higher. Furthermore, we analyzed the different gene expression of immunological checkpoints in different cluster groups. There was a significant reduction in the expression levels of most immune checkpoints in patients from cluster 2 compared to those in other subgroups (Figure 3G).

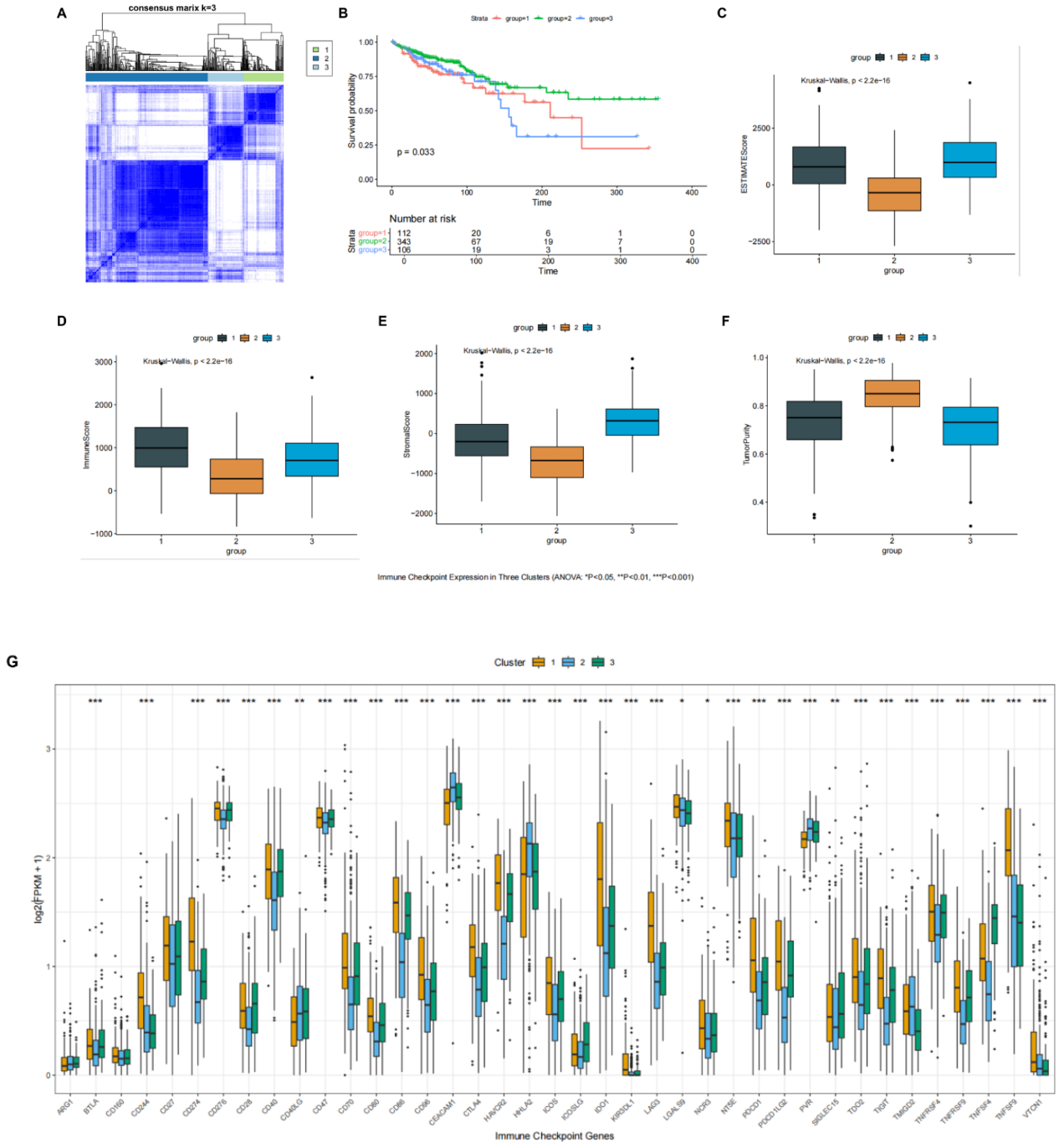

Figure 3. Molecular subtypes based on differentially expressed metabolism-related genes (MRGs) and immune-related genes (IRGs). This figure presents the consensus clustering matrix heatmap (k = 3) defining three metabolism–immune-related gene (MIRG) clusters, along with Kaplan–Meier survival curves showing significant overall survival differences across phenotypes (p = 0.033). Violin plots display the estimation of stromal and immune cells in malignant tumors using expression data (ESTIMATE) score, immune score, stromal score, and tumor purity for each phenotype, while box plots illustrate variations in immune checkpoint expression among clusters (*$p < 0.05$, **$p < 0.01$, ***$p < 0.001$).

Establishment and Validation of MIRGs

The development of a prognosis model based on manganese metabolism and immune response involved using univariate Cox regression analysis to find potential prognostic genes associated with overall survival in CRC patients from the TCGA cohort. Subsequently, eleven crucial genes were selected after refining the gene signature through LASSO regression analysis (Figures 4A-B). Based on the expression levels of these genes and their respective coefficients, a prognostic risk score for each CRC patient was calculated using the formula: RiskScore = (0.208 × *MPP2*) + (0.247 × *MC1R*) + (0.128 × *MAP2*) + (0.068 × *CALB2*) + (0.200 × *ALPP*) + (0.253 × *TERT*) + (-0.015 × *NAT2*) + (0.048 × *INHBB*) + (0.122 × *AQP7*) + (0.284 × *SEMA3E*) + (0.044 × *UCN*). The LASSO model was optimized using 10-fold cross-validation, which ensured model stability and reduced the risk of overfitting. Robustness of the prognostic signature was further confirmed in the independent GSE17538 cohort.

The TCGA-CRC database was used to stratify patients in the training set into high- and low-risk categories, using the median risk score as the threshold. According to Kaplan-Meier analysis, patients at high risk experienced notably shorter overall survival and increased mortality rates than those at low risk (p<0.001; Figure 4C). Figures 4D and 4E illustrate the distribution of survival status and risk scores within the cohort. Similarly, deceased individuals had elevated risk scores compared to survivors in the TCGA cohort. Figure 4F displays differential expression of the 11 signature genes between risk subgroups. ROC analysis was used to evaluate the prognostic effectiveness of this 11-gene signature, which produced an AUC of 0.685 for predicting overall survival (Figure 4G).

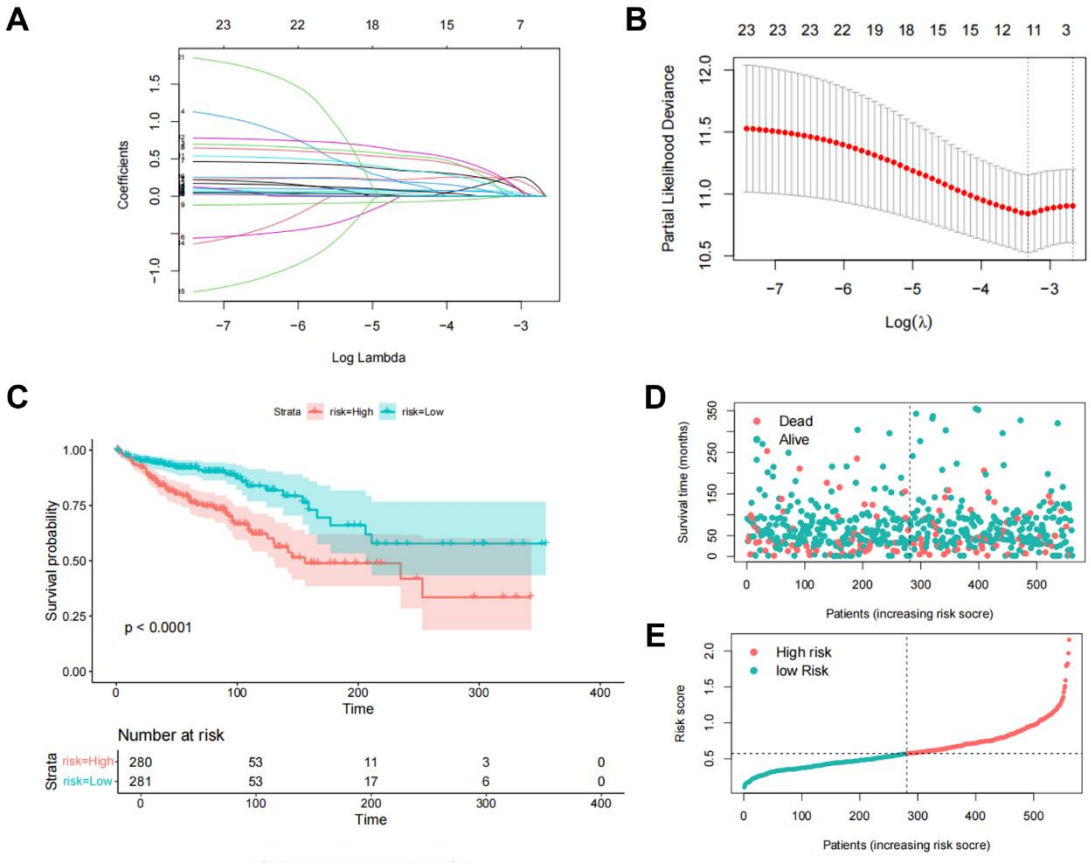

Published by Tehran University of Medical Sciences (http://ijaai.tums.ac.ir)

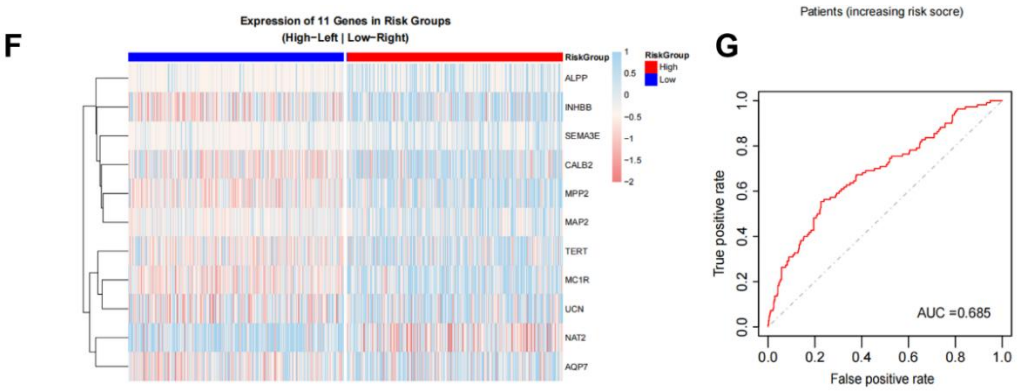

Figure 4. Construction and verification of metabolism–immune-related genes (MIRGs). This figure illustrates the development and validation of the MIRG signature, beginning with least absolute shrinkage and selection operator (LASSO) regression analysis (A–B), which identified 11 MIRG signature genes. The Kaplan–Meier survival curves (C) demonstrate significant survival stratification between high- and low-risk subgroups in The Cancer Genome Atlas (TCGA) cohort. Survival status distribution (D) and risk score distribution (E) further depict prognostic separation across patients. Heatmaps (F) show the expression patterns of the 11 MIRG genes within the TCGA cohort, and receiver operating characteristic (ROC) curves (G) evaluate the predictive performance of the MIRG signature for patient outcomes.

To validate the prognostic signature obtained from the TCGA dataset, the same risk score formula and median cutoff were applied to the independent GSE17538 CRC cohort. In this validation cohort, patients were also categorized into high-risk and low-risk subgroups. Aligning with the training set findings, those in the high-risk category had worse survival outcomes compared to the low-risk group (p=0.032). According to the Kaplan-Meier survival analysis, risk scores in the GSE17538 cohort were higher in deceased patients compared to the survival group. Moreover, the AUC of this 11-gene signature for overall survival prediction in the validation set was 0.616. To enhance clinical utility, we constructed nomograms incorporating the risk score and other prognostic factors (Figures 5A-B). Total nomogram scores inversely correlated with predicted survival probabilities at 12, 24, and 36 months.

Immunological Features of MIRGs

Immune landscape analysis revealed significant enrichment of macrophages, TGF-β signaling, and Treg cells in high-risk individuals in TCGA database (Figure 5C). Further immune profiling demonstrated increased activity of angiogenesis, apoptosis, EMT, M0/M2 macrophages, Notch signaling, and TGF-β signaling in the high-risk subgroup (Figure5D), indicating distinct immunological characteristics between risk groups.

Exploring MIRGs' Biological Functions

We examined the differences in biological functions associated with prognosis between high-risk and low-risk groups by performing a functional enrichment analysis. GSEA with GO gene sets demonstrated that low-risk patients were significantly enriched in metabolism and detoxification pathways, including HALLMARK OXIDATIVE PHOSPHORYLATION, HALLMARK MYC TARGETS V1, HALLMARK MYOGENESIS, HALLMARK FATTY ACID METABOLISM, and HALLMARK PEROXISOME (Figure 6A-B). Alternatively, high-risk patients revealed substantial enrichment in pathways linked to cancer, such as HALLMARK KRAS SIGNALING. Furthermore, through GSVA based on Hallmark gene sets, we confirmed that the high-risk group exhibited stronger activation in pathways associated with HALLMARK APICAL SURFACE, HALLMARK APICAL JUNCTION, HALLMARK EPITHELIAL MESENCHYMAL TRANSITION, and HALLMARK ANGIOGENESIS. In contrast, the low-risk group showed significantly activity in pathways such as HALLMARK SPERMATOGENESIS (Figure 6C). Risk scores significantly correlated with hallmark pathway activities (Figure 6D), suggesting biological relevance. Survival analysis linked favorable prognosis to HALLMARK_BILE_ACID_METABOLISM and HALLMARK_PEROXISOME (Figures 6E-F), while HALLMARK_KRAS_SIGNALING and HALLMARK_MYOGENESIS associated with poor outcomes.

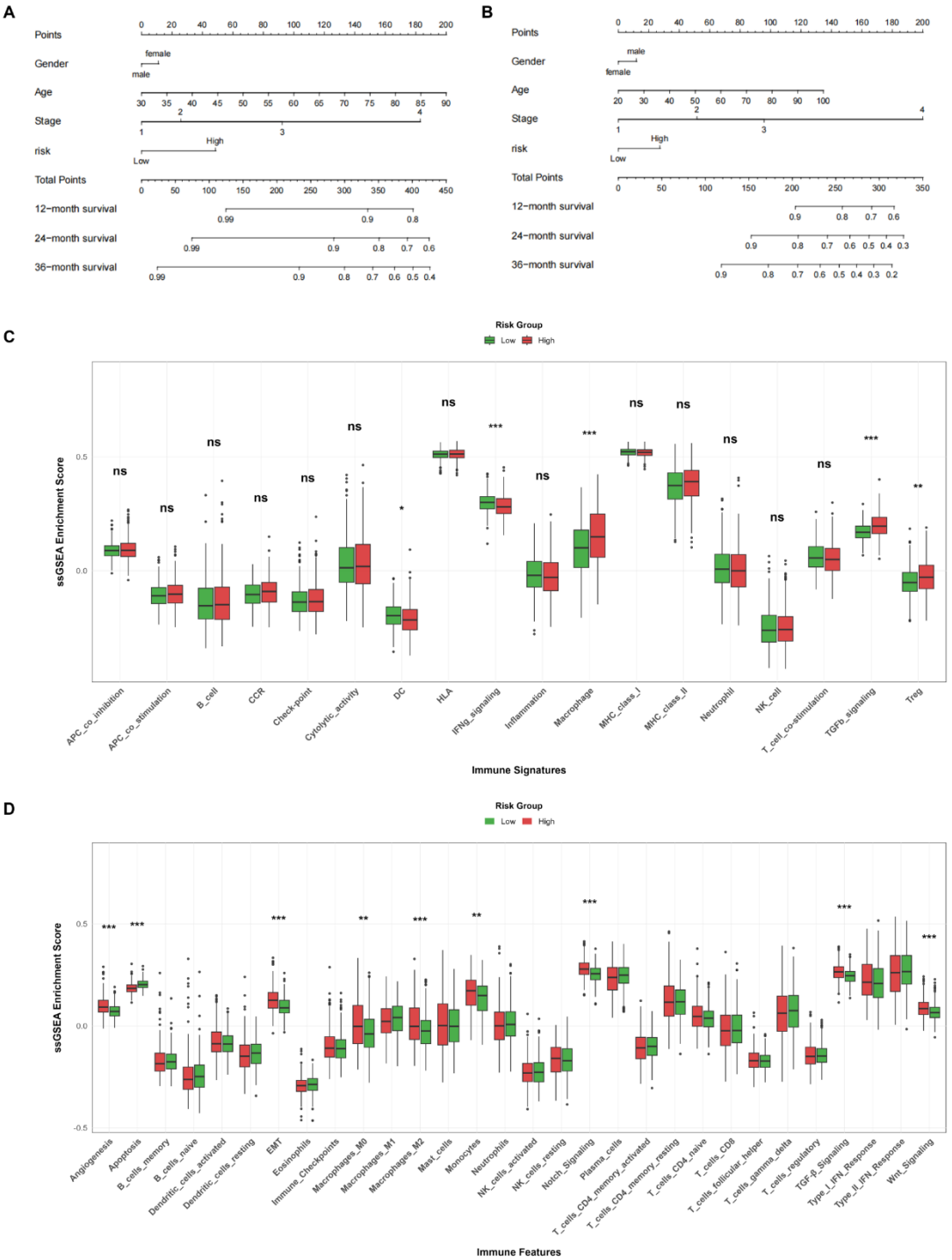

Figure 5. Development of nomograms based on clinical features and risk scores. This figure presents nomograms predicting 12-, 24-, and 36-month survival probabilities for colorectal cancer (CRC) patients in The Cancer Genome Atlas (TCGA) cohort (A) and the Gene Expression Omnibus (GEO) cohort (B). Comparative analyses illustrate differences in immune cell infiltration (C) and immune function (D) between high- and low-risk strata, highlighting immunological divergence associated with the risk model.

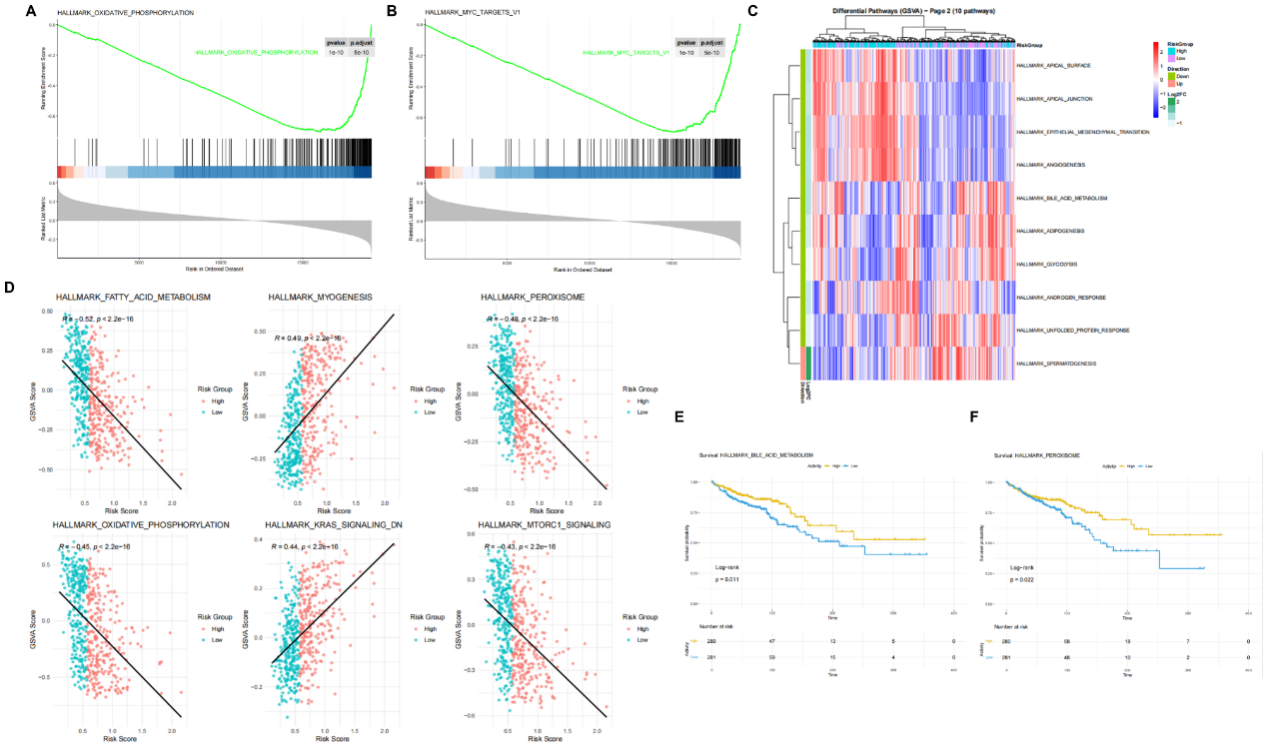

Figure 6. Transcriptomic characteristics of metabolism–immune-related gene (MIRG)–stratified colorectal cancer (CRC) patients. This figure depicts differences in pathway activity between risk groups using Gene Set Variation Analysis (GSVA), with panels A–B showing hallmark pathway activity disparities and panel C presenting a heatmap of GSVA-scored hallmark pathways across risk strata. Panel D displays correlations between MIRG-derived risk scores and GSVA-quantified pathway activities. Kaplan–Meier analyses in panels E–F illustrate overall survival (OS) associations with GSVA scores for the HALLMARK BILE ACID METABOLISM and HALLMARK PEROXISOME pathways, highlighting biologically meaningful metabolic variations between patient groups.

Somatic Mutation Analysis

TMB analysis revealed differential mutation patterns between risk groups. The distributions of variant classifications, types, and SNV classes for high-risk and low-risk patients are depicted in Figures 7A-F. Patients at high risk demonstrated higher TMB and unique mutation patterns, as illustrated by the top 10 mutated genes (Figures 7G-H) and the waterfall plots of the top 30 most frequently mutated genes (Figures 7I-J). Patients classified as high-risk demonstrate a significantly higher mutation burden (p<0.001), as revealed by mutation feature analysis.

The mRNA Expression of Eleven Genes from MIRGs in Colorectal Tissues

Figure 8A demonstrates significant expression differences for eleven genes from MIRGs between tumor and normal tissues in the TCGA-CRC cohort. Comparative analysis of mRNA expression revealed dysregulation of most MIRGs in 50 CRC tissues relative to adjacent normal tissues, consistent with TCGA data. Specifically, tumor tissues exhibited significantly elevated expression of *MC1R*, *INHBB*, and *UCN* (Figure 8B). Conversely, *MPP2*, *CALB2*, *NAT2*, *AQP7*, and *SEMA3E* showed marked downregulation in CRC specimens (Figure 8B). These findings implicate these MIRGs in colorectal carcinogenesis. Interestingly, *MAP2*, *ALPP*, and *TERT* did not show significant differences in expression between tumor and corresponding normal tissues in our study, which contrasts with TCGA findings.

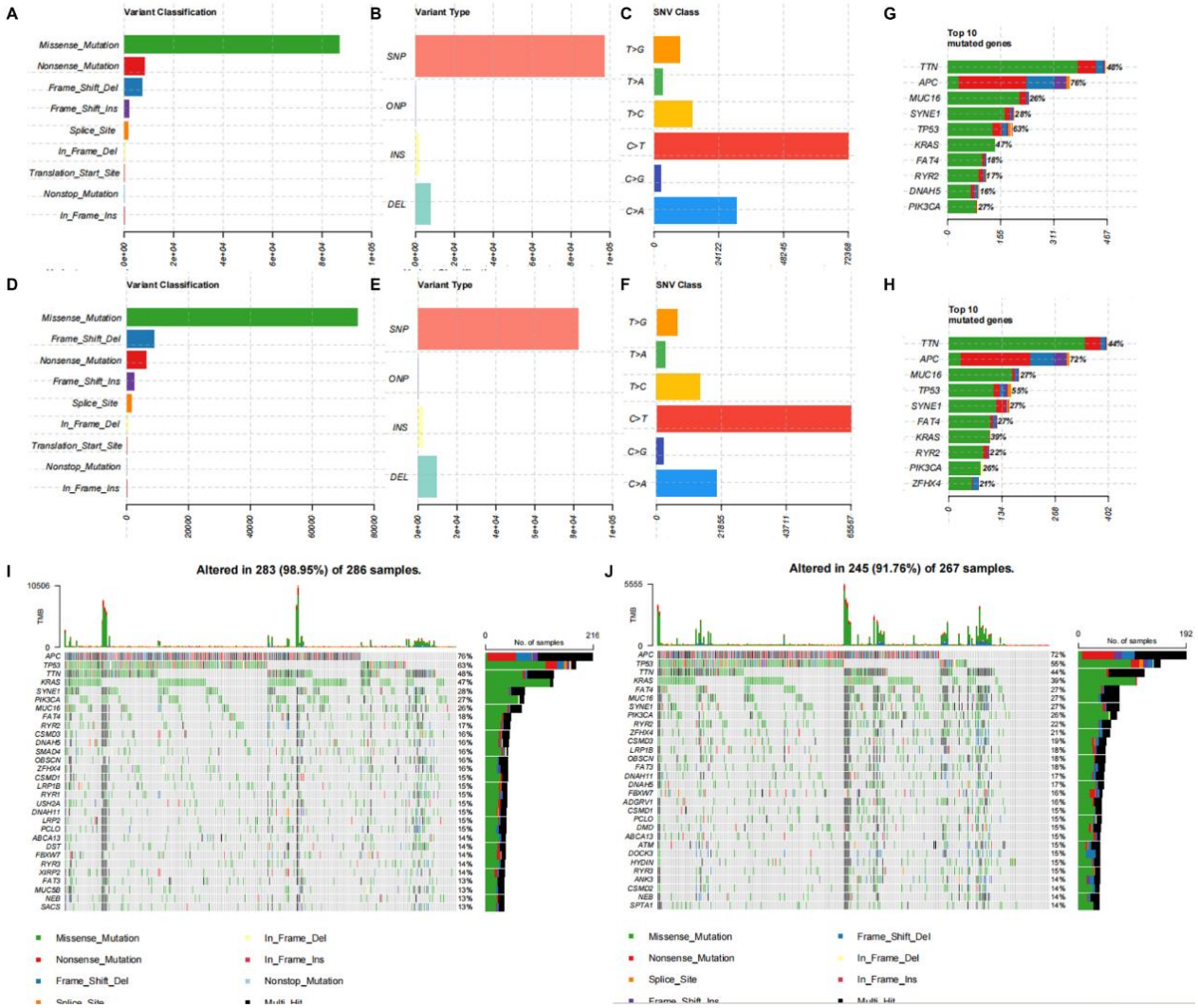

Figure 7. Evaluation of tumor mutational burden (TMB) between MIRG-defined risk subgroups. This figure characterizes genomic alterations across risk groups, beginning with the distribution of variant classifications in the high-risk subgroup (A) and the composition of genomic alteration types within this group (B), followed by the spectrum of single-nucleotide substitution patterns (C). Panels D–F depict the corresponding variant classifications, alteration type composition, and substitution spectrum in the low-risk subgroup. Panels G–H highlight the top ten most frequently mutated genes in the high-risk and low-risk groups, respectively. Waterfall plots in panels I–J illustrate the detailed mutation landscapes of individual patients in each subgroup, underscoring mutational heterogeneity associated with metabolism–immune-related gene–based risk stratification.

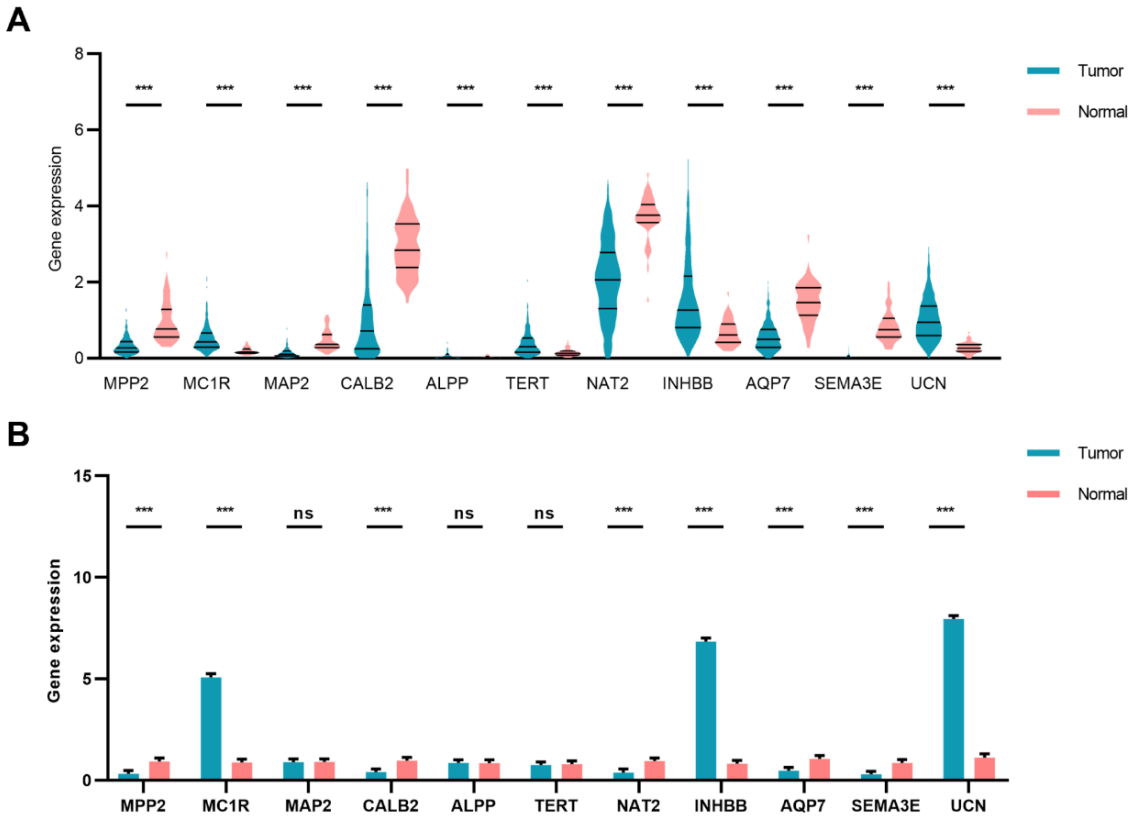

Figure 8. Expression of the 11 metabolism–immune-related gene (MIRG) signature genes in human colorectal tissues. This figure illustrates gene expression patterns using data from The Cancer Genome Atlas (TCGA) (A) and from in-house clinical colorectal cancer (CRC) specimens (B), showing differential expression across tumor and normal tissues with significance levels indicated (*$p < 0.05$, **$p < 0.01$, ***$p < 0.001$).

DISCUSSION

Globally, CRC is a primary cause of cancer-related deaths, marked by considerable genetic variability and common late-stage detection.[17] Despite the promise of immunotherapy, its success is limited to a small number of tumors with high microsatellite instability, resulting in about 95% of metastatic CRC (mCRC) patients with proficient mismatch repair or non-MSI-H being unresponsive to current immunotherapy treatments.[18] Recent advances highlight the cGAS-STING pathway as pivotal in anti-tumor immunity, with manganese serving as a key activator that enhances cGAS-STING signaling and synergizes with ICIs.[19] This synergy was exemplified by manganese galvanic cells, which modulate tumor metabolism to boost cGAS-STING activation and improve hydrogen-immunotherapy efficacy in preclinical CRC models.[20] These findings underscore the clinical potential of integrating manganese metabolism and immunity to overcome immunotherapy resistance in CRC.

Bioinformatics advances have enabled prognostic models based on immune signatures, yet few integrate biological factors like manganese metabolism. Our study bridges this gap by combining MIRGs to refine prognostic stratification. Functional enrichment revealed MIRGs are involved in immune activation pathways, including cytokine-cytokine receptor interactions, IL-17 signaling, and leukocyte migration.[21,22] Through unsupervised clustering, we identified three molecular subtypes with distinct survival outcomes, where Cluster 2 exhibited a superior prognosis despite lower immune scores and higher tumor purity. These results suggest favorable outcomes may stem from attenuated pro-tumor immunosuppression rather than enhanced anti-tumor immunity which was corroborated by suppressed immune checkpoint expression in Cluster 2.[23,24]

Additional examination discovered distinct immune checkpoint and enrichment pathway patterns in these subtypes, underscoring their prognostic impact. The analysis resulted in the creation of a novel prognostic signature, MIRGs, which incorporates eleven genes: *MPP2*, *MC1R*, *MAP2*, *CALB2*, *ALPP*, *TERT*, *NAT2*, *INHBB*, *AQP7*, *SEMA3E*, and *UCN*. MIRGs were effective in classifying CRC patients into high-risk and low-risk categories. Patients at high risk showed notably reduced overall survival and lower survival rates. Additionally, MIRGs served as an independent prognostic marker for CRC patient outcomes. The construction of nomograms that incorporate the risk score alongside multiple clinical variables allows for a comprehensive evaluation of the prognostic utility of MIRGs. This work presents an innovative integration of MRGs with IRGs, providing a distinct prognostic model and suggesting potential therapeutic strategies for CRC.

We delved deeper into the molecular mechanisms underlying the significant prognostic differences among diverse risk subgroups in CRC. Investigations into immune cell infiltration uncovered a considerable percentage of M0/M2 macrophages, as well as Notch and TGF-β signaling, within the high-risk subgroup.[25] Macrophages, derived from monocytes, are categorized into M1 and M2 subtypes.[26] Prior research has shown that M2 macrophages play a crucial role in the development and progression of CRC.[27] Increasing consensus suggests that M2 macrophage infiltration is strongly linked to the immune evasion microenvironment in CRC.

The secretion of pro-angiogenic molecules such as transforming growth factor-α, transforming growth factor-β, and vascular endothelial growth factor by M2 macrophages promotes angiogenesis in CRC. Through the induction of EMT, M2 macrophages support the migration and infiltration of tumor cells in CRC.[28,29] Moreover, by secreting *CHI3L1*, M2 macrophages trigger CRC metastasis and contribute to the advancement of CRC by influencing metabolism, particularly in relation to fatty acids, arginine, proline, and methionine metabolism. The presence of a high density of M2 macrophages is known to predict poor outcomes in CRC.[30] Our study also found a significant abundance of M2 macrophages in patients at high risk with tumor progression and negative prognoses. In addition to M2 macrophages, the high-risk microenvironment was also characterized by an enrichment of Tregs and a relative deficiency in cytotoxic $CD8^+$ T cells, fostering an overall immunosuppressive state.

According to GSVA, the high-risk group demonstrated enrichment in pathways associated with cancer, including EMT, angiogenesis, KRAS, apical surface, and apical junction. Previous studies demonstrated the EMT pathway facilitates CRC metastasis by downregulating epithelial markers such as *E-cadherin* while upregulating mesenchymal proteins including *Vimentin*.[31] This process enhances tumor cell detachment from primary sites and promotes invasive potential particularly within microsatellite unstable subtypes. Dysregulated angiogenesis driven by *DDX21*-mediated acetylation modifications stabilizes pro-angiogenic transcripts like *VEGF* and induces abnormal vascular networks that accelerate hepatic metastasis and peritoneal dissemination in CRC.[32] Additionally, *KRAS* signaling activation, specifically the G13D mutation variant, recruits immunosuppressive Treg cells at tumor invasive fronts through JNK pathway activation, thereby establishing immunotherapy resistance in metastatic CRC.[33] Apical surface and junction integrity disruption occurs through lipid raft-localized Src kinase activation which subverts epithelial extrusion mechanisms and initiates early stromal invasion in colorectal carcinogenesis.[34] These particular molecular processes may shed light on the unfavorable prognosis seen in high-risk CRC patients.

Notably, previous studies have observed dysregulation of MIRGs underscores their potential involvement in the pathogenesis of several cancer, including gastric cancer[35] and kidney cancer.[36] In this study, we analyzed the mRNA expression of eleven MIRGs genes using qRT-PCR on fifty pairs of CRC and nearby non-tumor tissues. Our research identified the dysregulation of most MIRGs in CRC tissues relative to adjacent normal tissues, consistent with TCGA data. As a result, MIRGs are highly promising as a therapeutic and prognostic indicator in CRC. Collectively, our tissue-level validation confirms the consistent dysregulation of these MIRGs in CRC pathogenesis and positions them as promising candidates for diagnostic and therapeutic targeting across gastrointestinal malignancies.

In summary, this research developed a new prognostic model for CRC that includes eleven genes related to manganese metabolism and the immune system. The model showed strong predictive accuracy for patient outcomes, improving clinical risk assessment. A promising strategy for overcoming

resistance to immunotherapy in advanced diseases is the integration of manganese-based agents with immune checkpoint inhibitors. However, their clinical translation will depend on future studies assessing the safety and efficacy of such combinations in patients. Due to the limited sample size of MSI-H cases in this cohort, a stratified analysis by MSI status was not statistically feasible. In addition, several limitations warrant consideration, including reliance on public databases and in-house qRT-PCR validation. The generalizability of our findings is constrained by the relatively small sample size and single-center design of our validation cohort, necessitating further confirmation in larger, multi-center studies. Preclinical validation in cellular and animal systems remains essential prior to clinical implementation.

STATEMENT OF ETHICS

This study obtained approval from the independent Ethics Committee of Nanjing Hospital of Chinese Medicine, affiliated with Nanjing University of Chinese Medicine (KY2024010).

FUNDING

Not applicable.

CONFLICT OF INTEREST

The authors declare that the research was conducted in the absence of any commercial or financial relationships that could be construed as a potential conflict of interest.

ACKNOWLEDGMENTS

We would like to acknowledge the TCGA and the GEO (GSE17538) for providing data.

DATA AVAILABILITY

The original contributions presented in the study are included in the article; further inquiries can be directed to the corresponding author.

AI ASSISTANCE DISCLOSURE

Not applicable.

REFERENCES

1. Siegel RL, Kratzer TB, Giaquinto AN, Sung H, Jemal A. Cancer statistics, 2025. Ca-Cancer J Clin. 2025;75(1):10-45.
2. Wagle NS, Nogueira L, Devasia TP, Mariotto AB, Yabroff KR, Islami F, et al. Cancer treatment and survivorship statistics, 2025. Ca-Cancer J Clin. 2025;75(4):308-40.
3. Weng J, Li S, Zhu Z, Liu Q, Zhang R, Yang Y, et al. Exploring immunotherapy in colorectal cancer. J Hematol Oncol. 2022;15(1):95.
4. Shin AE, Giancotti FG, Rustgi AK. Metastatic colorectal cancer: mechanisms and emerging therapeutics. Trends Pharmacol Sci. 2023;44(4):222-36.
5. Li J, Wu C, Hu H, Qin G, Wu X, Bai F, et al. Remodeling of the immune and stromal cell compartment by PD-1 blockade in mismatch repair-deficient colorectal cancer. Cancer Cell. 2023;41(6):1152-69.
6. Wang X, Fang Y, Liang W, Wong CC, Qin H, Gao Y, et al. Fusobacterium nucleatum facilitates anti-PD-1 therapy in microsatellite stable colorectal cancer. Cancer Cell. 2024;42(10):1729-46.
7. Andre T, Shiu KK, Kim TW, Jensen BV, Jensen LH, Punt C, et al. Pembrolizumab in Microsatellite-Instability-High Advanced Colorectal Cancer. New Engl J Med. 2020;383(23):2207-18.
8. Kwon J, Bakhoum SF. The Cytosolic DNA-Sensing cGAS-STING Pathway in Cancer. Cancer Discov. 2020;10(1):26-39.
9. Zhang Z, Zhang C. Regulation of cGAS-STING signalling and its diversity of cellular outcomes. Nat Rev Immunol. 2025;25(6):425-44.
10. Lv M, Chen M, Zhang R, Zhang W, Wang C, Zhang Y, et al. Manganese is critical for antitumor immune responses via cGAS-STING and improves the efficacy of clinical immunotherapy. Cell Res. 2020;30(11):966-79.
11. Wang Y, Wu M, Wang X, Wang P, Ning Z, Zeng Y, et al. Biodegradable MnO(2)-based gene-engineered nanocomposites for chemodynamic therapy and enhanced antitumor immunity. Mater Today Bio. 2023;18:100531.
12. Zhang K, Qi C, Cai K. Manganese-Based Tumor Immunotherapy. Adv Mater. 2023;35(19):e2205409.
13. Wang Y, Fan N, Wang R, Li X, Zhao F, Miao L, et al. Discovery of Airway-Administered Ionophores for Mn(2+) to Mitigate Lung Metastasis by Targeting Disseminated Tumor Cell. Acs Nano. 2025;19(14):14330-50.
14. Peng Y, Liang S, Liu D, Ma K, Yun K, Zhou M, et al. Multi-Metallic Nanosheets Reshaping Immunosuppressive Tumor Microenvironment through Augmenting cGAS-STING Innate Activation and Adaptive Immune

Responses for Cancer Immunotherapy. Adv Sci. 2024;11(38):e2403347.
15. Fu Y, Liu S, Zeng S, Shen H. From bench to bed: the tumor immune microenvironment and current immunotherapeutic strategies for hepatocellular carcinoma. J Exp Clin Canc Res. 2019;38(1):396.
16. Galon J, Bruni D. Approaches to treat immune hot, altered and cold tumours with combination immunotherapies. Nat Rev Drug Discov. 2019;18(3):197-218.
17. Feng X, Zahed H, Onwuka J, Callister M, Johansson M, Etzioni R, et al. Cancer Stage Compared With Mortality as End Points in Randomized Clinical Trials of Cancer Screening: A Systematic Review and Meta-Analysis. Jama-J Am Med Assoc. 2024;331(22):1910-7.
18. Fan A, Wang B, Wang X, Nie Y, Fan D, Zhao X, et al. Immunotherapy in colorectal cancer: current achievements and future perspective. Int J Biol Sci. 2021;17(14):3837-49.
19. Yang N, Sun S, Xu J, Gong F, Lei H, Hao Y, et al. Manganese Galvanic Cells Intervene in Tumor Metabolism to Reinforce cGAS-STING Activation for Bidirectional Synergistic Hydrogen-Immunotherapy. Adv Mater. 2025;37(8):e2414929.
20. Liang Q, Chen J, Hou S, Li D, Zhu Y, Li R, et al. Activatable Mn(2+)-Armed nanoagonist augments antitumor immunity in colorectal cancer: A NIR-II Photonic neoadjuvant paradigm. Biomaterials. 2023;300:122206.
21. Ngo U, Shi Y, Woodruff P, Shokat K, DeGrado W, Jo H, et al. IL-13 and IL-17A activate beta1 integrin through an NF-kB/Rho kinase/PIP5K1gamma pathway to enhance force transmission in airway smooth muscle. P Natl Acad Sci Usa. 2024;121(34):e1893716175.
22. Neeli I, Moarefian M, Kuseladass J, Dwivedi N, Jones C, Radic M. Neutrophil attachment via Mac-1 (alpha(M)beta(2); CD11b/CD18; CR3) integrins induces PAD4 deimination of profilin and histone H3. Philos T R Soc B. 2023;378(1890):20220247.
23. Chow A, Perica K, Klebanoff CA, Wolchok JD. Clinical implications of T cell exhaustion for cancer immunotherapy. Nat Rev Clin Oncol. 2022;19(12):775-90.
24. Ambrosini M, Rousseau B, Manca P, Artz O, Marabelle A, Andre T, et al. Immune checkpoint inhibitors for POLE or POLD1 proofreading-deficient metastatic colorectal cancer. Ann Oncol. 2024;35(7):643-55.
25. Mao X, Xu J, Wang W, Liang C, Hua J, Liu J, et al. Crosstalk between cancer-associated fibroblasts and immune cells in the tumor microenvironment: new findings and future perspectives. Mol Cancer. 2021;20(1):131.
26. Chen S, Saeed A, Liu Q, Jiang Q, Xu H, Xiao GG, et al. Macrophages in immunoregulation and therapeutics. Signal Transduct Tar. 2023;8(1):207.
27. Zhao S, Mi Y, Guan B, Zheng B, Wei P, Gu Y, et al. Tumor-derived exosomal miR-934 induces macrophage M2 polarization to promote liver metastasis of colorectal cancer. J Hematol Oncol. 2020;13(1):156.
28. Liu X, Wang X, Yang Q, Luo L, Liu Z, Ren X, et al. Th17 Cells Secrete TWEAK to Trigger Epithelial-Mesenchymal Transition and Promote Colorectal Cancer Liver Metastasis. Cancer Res. 2024;84(8):1352-71.
29. Yang PS, Yu MH, Hou YC, Chang CP, Lin SC, Kuo IY, et al. Targeting protumor factor chitinase-3-like-1 secreted by Rab37 vesicles for cancer immunotherapy. Theranostics. 2022;12(1):340-61.
30. Hong SM, Lee AY, Kim BJ, Lee JE, Seon SY, Ha YJ, et al. NAMPT-Driven M2 Polarization of Tumor-Associated Macrophages Leads to an Immunosuppressive Microenvironment in Colorectal Cancer. Adv Sci. 2024;11(14):e2303177.
31. Zhang Y, Yang Y, Qi X, Cui P, Kang Y, Liu H, et al. SLC14A1 and TGF-beta signaling: a feedback loop driving EMT and colorectal cancer metachronous liver metastasis. J Exp Clin Canc Res. 2024;43(1):208.
32. Song A, Liu B, Li W, Chen B, Gui P, Zhang H, et al. Competitive binding between DDX21 and SIRT7 enhances NAT10-mediated ac(4)C modification to promote colorectal cancer metastasis and angiogenesis- DDX21 promotes colorectal cancer metastasis. Cell Death Dis. 2025;16(1):353.
33. Huang J, Gong Q, Li Q, Xiao M, Li M, Zhang S, et al. Analysis of the immune microenvironment in colorectal cancer with different KRAS gene subtypes. Bmc Cancer. 2025;25(1):1267.
34. Ruiz-Saenz A, Atreya CE, Wang C, Pan B, Dreyer CA, Brunen D, et al. A reversible SRC-relayed COX2 inflammatory program drives resistance to BRAF and EGFR inhibition in BRAF(V600E) colorectal tumors. Nat Cancer. 2023;4(2):240-56.
35. Han X, Leng C, Zhao S, Wang S, Chen S, Wang S, et al. Development and verification of a manganese metabolism- and immune-related genes signature for prediction of prognosis and immune landscape in gastric cancer. Front Immunol. 2024;15:1377472.
36. Liu Y, Ye H, Zhang R, Liu X, Liu R. A manganese metabolism-related gene signature stratifies prognosis and immunotherapy efficacy in kidney cancer. Discov Oncol. 2025;16(1):1242.